Evaluation of irradiation hardening of ion-irradiated V-4Cr-4Ti and V-4Cr-4Ti-0.15Y alloys by nanoindentation techniques

ID: 16-472

Evaluation of irradiation hardening of ion-irradiated V-4Cr-4Ti and V-4Cr-4Ti-0.15Y alloys by nanoindentation techniques

Takeshi Miyazawa[a,*], Takuya Nagasaka[a,b], Ryuta Kasada[c], Yoshimitsu Hishinuma[a,b], Takeo Muroga[a,b], Hideo Watanabe[d], Takuya Yamamoto[e], Shuhei Nogami[f] and Masahiko Hatakeyama[g]

[a] The Graduate University for Advanced Studies, Oroshi, Toki, Gifu 509-5292, Japan

[b] National Institute for Fusion Science, Oroshi, Toki, Gifu 509-5292, Japan

[c] Institute of Advanced Energy, Kyoto University, Uji, Kyoto 611-0011, Japan

[d] Research Institute for Applied Mechanics, Kyushu University, Kasuga-kouen, Kasugashi, Fukuoka 816-8580, Japan

[e] Department of Mechanical and Environmental Engineering, UC Santa Barbara, Santa Barbara, CA 93106, USA

[f] Department of Quantum Science and Energy Engineering, Tohoku University, Aramaki-aza-Aoba, Aoba-ku, Sendai 980-8579, Japan

[g] International Research Center for Nuclear Materials Science, IMR/Tohoku University, Narita, Oarai, Ibaraki 311-1313, Japan

* Corresponding author, Tel. +81-572-58-2332, Fax. +81-572-58-2676, email: miyazawa.takeshi@LHD.nifs.ac.jp

Abstract:

Irradiation hardening behavior of V-4Cr-4Ti and V-4Cr-4Ti-0.15Y alloys after Cu-ion beam irradiation were investigated with a combination between nanoindentation techniques and finite element method (FEM) analysis. The ion-irradiation experiments were conducted at 473 K with 2.4 MeV Cu^{2+} ions up to 7.6 dpa. For the unirradiated materials, the increase in nanoindentation hardness with decreasing indentation depth, so-called indentation size effect (ISE), was clearly observed. After irradiation, irradiation hardening in the measured depth was identified. Hardening behavior of bulk-equivalent hardness for V-4Cr-4Ti-0.15Y alloy was similar to that for V-4Cr-4Ti alloy. Y addition has little effect on irradiation hardening at 473 K. Adding the concept of geometrically necessary dislocations (GNDs) to constitutive equation of V-4Cr-4Ti alloy, the ISE was simulated. A constant value of $\alpha = 0.5$ was derived as an optimal value to simulate nanoindentation test for ion-irradiated V-4Cr-4Ti alloy. Adding the term of irradiation hardening $\Delta\sigma_{irrad.}$ to constitutive equation with $\alpha = 0.5$, FEM analyses for irradiated surface of V-4Cr-4Ti alloy were carried out. The analytic data of FEM analyses based on neutron-irradiation hardening equivalent to 3.0 dpa agreed with the experimental data to 0.76 dpa. The comparison indicates that irradiation hardening by heavy ion-irradiation is larger than that by neutron-irradiation at the same displacement damage level. Possible mechanisms for extra hardening by heavy ion-irradiation are the processes that the injected Cu ions could effectively produce irradiation defects such as interstitials compared with neutrons, and that higher damage rate of ion-irradiation enhanced

nucleation of irradiation defects and hence increased the number density of the defects compared

with neutron-irradiation.

Main text:

Evaluation of irradiation hardening of ion-irradiated V-4Cr-4Ti and V-4Cr-4Ti-0.15Y alloys by nanoindentation techniques

Takeshi Miyazawa, Takuya Nagasaka, Ryuta Kasada, Yoshimitsu Hishinuma, Takeo Muroga, Hideo Watanabe, Takuya Yamamoto, Shuhei Nogami and Masahiko Hatakeyama

1. Introduction

Low-temperature irradiation embrittlement determines the operation temperature limit of V-4Cr-4Ti alloys for the application to structural materials of fusion reactors [1, 2]. The embrittlement is known to be enhanced by irradiation defects decorated by interstitial oxygen. In order to improve the irradiation embrittlement, yttrium (Y) was added to reduce the interstitial oxygen due to the formation of Y_2O_3. It has been reported that Y addition was effective to improve ductility after neutron-irradiation [3, 4], while neutron-irradiation data are too few to prove how much Y addition is effective in irradiation condition of lower temperature region and of high-dose [5]. The effect of Y addition on irradiation hardening in lower temperature region and at high-dose was still unsolved.

To simulate fusion neutron irradiation damage in structural materials, the heavy ion-irradiation experiments have been carried out because of the rapid damage production and the absence of induced radioactivity [6]. The heavy ion-irradiation experiments also have some

problems such as the shallow damage profiles. Conventional mechanical tests are difficult to measure the irradiation hardening on the limited surface area. A nanoindentation test is capable of measuring mechanical properties on the ion-irradiated surface because of the highly-accurate depth-sensing loading method. Nevertheless, it has been difficult to quantitatively evaluate the irradiation hardening for the ion-irradiated surface because the increase in the hardness of materials, so-called indentation size effect (ISE) [7], is observed even in the unirradiated surface. One of the author (RK) [8] has developed an experimental analysis models to estimate the bulk-equivalent hardness by extending Nix-Gao model [7] in order to explain the ISE. RK model enables to convert the nanoindentation hardness of ion-irradiated materials into the bulk-equivalent hardness which is related to Vickers hardness. However, it is necessary to estimate the damage gradient effect (DGE) due to the damage profile in the ion-irradiated materials. In the present paper, an optimization between nanoindentation test results and finite element method (FEM) analysis estimates depth profiles of irradiation hardening in the shallow depth for the ion-irradiated materials. In addition, it discusses the correlation between neutron-irradiation and heavy ion-irradiation from the viewpoint of mechanical strength.

2. Experiment

2.1. Specimens and ion-irradiation conditions

Two type vanadium alloys were used in this study; one was the reference V-4Cr-4Ti alloy, NIFS-HEAT-2, which was fabricated by electron beam melting and vacuum arc re-melting in 166 kg-scale [9]. NIFS-HEAT-2 is high-purity large scale ingots developed by National Institute for Fusion Science, Japan. The other was a high-purity V-4Cr-4Ti-0.15Y alloy fabricated by a levitation melting process in 15 kg-scale [10]. Disk specimens with $\phi 3$ x 0.25 mm in size were prepared for nanoindentation test. After mechanical polishing and electro-polishing, the specimens were annealed at 1273 K for 7.2 ks for V-4Cr-4Ti alloy, and at 1223 K for 3.6 ks for the V-4Cr-4Ti-0.15Y alloy in a vacuum better than 1 x 10^{-4} Pa. Ion-irradiation experiments were performed with 2.4 MeV Cu^{2+} ions at 473 K using a tandem type accelerator at RIAM Kyusyu University. Depth profiles of the displacement rate and Cu ions deposition rate were calculated by the SRIM code with full-cascade options [11], as shown in Fig. 1. Figure 1 shows a simulation of 2.4 MeV Cu^{2+} ions incident on a pure V target with the displacement threshold energy of 40 eV [12]. The nominal displacement rate was defined as 1.8 x 10^{-4} dpa/s at damage peak (800 nm). Depth profile of the deposition rate has a peak at a depth of about 1000 nm.

2.2. Nanoindentation tests

Nanoindentation tests were performed using a Nano Indenter G200 (Agilent Technologies) with Berkovich type indentation tip. The continuous stiffness measurement (CSM) was used to continuously obtain nanoindentation hardness (*H*) vs. indentation depth (*h*) profile up to a depth of about 1000 nm. The nominal strain rate was 0.05 s^{-1}. The distance between indentations was about 50 μm. The calibration of the bluntness of the indentation tip is based on the Oliver-Pharr method [13].

2.3. Finite element modeling

The nanoindentations were modeled as a two-dimensional axisymmetric model using the commercial finite element program, ANSYS. A movable elastic conical indenter which has 70.3º half-included tip angle, Young modulus of 1140 GPa and Poisson's ratio of 0.07 approximates the triangular Berkovich indenter. The indenter gives the same depth-to-area ratio ($A = 24.56h^2$) as the Berkovich pyramid used in the nanoindentation tests. Tip radius used in this study was 100 nm. In order to represent a high stress and strain gradient well, the element size decreased near the point of contact with the indenter. The size of a specimen was 100 (with) x 100 (height) μm, and the size of an element just under the indenter was 10 x 20 nm. The interaction between the indenter tip and the surface of a specimen is defined as a sliding surface with friction. A contact friction value of 0.15

was chosen, since it was shown that a friction coefficient varying from 0 to 1.0 had a negligible effect on the results [14].

Figure 2 shows uniaxial true stress - true plastic strain curves of V-4Cr-4Ti alloy tested at room temperature at an initial strain rate of 0.05 s^{-1}. The experimental tensile curve was approximated by Swift's empirical law [15] as follows:

$$\sigma_0(\varepsilon_{pl}) = 605\left(\varepsilon_{pl} + 0.037\right)^{0.17} \quad (1)$$

where ε_{pl} is the plastic strain. The curve was approximated to determine the strain hardening exponent $n = 0.17$ because of the relationship between the uniform elongation and the strain hardening exponent. The curve-fitting for true stress - true plastic strain curve after Ludas deformation, which is the equation; $\sigma_0(\varepsilon_{pl}) = 649(\varepsilon_{pl}+0.03)^{0.18}$, showed same analytic results within ±2 %. Considering the Ludas deformation had a negligible effect on the results. Young modulus of 129 GPa was quoted from a previous study [16].

3. Results and discussion

3.1. Nanoindentation hardness

Figure 3 plots depth profiles of the averaged nanoindentation hardness for (a) V-4Cr-4Ti

alloy and (b) V-4Cr-4Ti-0.15Y alloy before and after the ion-irradiation. For the unirradiated

materials, the increase in hardness with decreasing indentation depth was clearly observed at the

indentation depth of $h > 50$ nm. Such depth-dependent hardness behavior has been recognized and

defined as an indentation size effect (ISE) [7]. After the ion-irradiations, the nanoindentation

hardness increased at the measured indentation depth. Therefore, irradiation hardening was

identified. To explain ISE, the Nix-Gao model predicts the hardness profile as follows:

$$H(h) = H_0 \sqrt{1 + \frac{h^*}{h}} \qquad (2)$$

where H_0 is the hardness at infinite depth (i.e., bulk-equivalent hardness), and h^* is a characteristic

length which depends on the material and the shape of indenter tip. The averaged nanoindentation

hardness data were plotted as H^2 versus $1/h$ in Fig. 4. The hardness for the unirradiated materials

shows a good linearity in the range of $h > 100$ nm. The hardness for the ion-irradiated materials,

however, appear to have a bilinearity in the range of $h > 100$ nm with a shoulder at a critical

indentation depth (about 200-400 nm). Over the critical indentation depth, a contribution of softer

unirradiated region beyond the harder ion-irradiated region to the measured hardness cannot be

neglected with increasing the indentation depth. The unirradiated region will begin to deform

plastically before the indenter tip reaches the region. Kasada et al. have developed a model to

extrapolate the experimentally obtained nanoindentation hardness to the bulk-equivalent hardness of

ion-irradiated Fe-based binary alloys [8]. Using the experimental analysis model, the

bulk-equivalent hardness for V-4Cr-4Ti alloys before and after ion-irradiation was extrapolated

from the least squares fitting of hardness data of Eq. (2) in the range of 300-1000 nm for

unirradiated materials and of 100-200 nm for ion-irradiated materials. Figure 5 shows dose

dependence of bulk-equivalent hardness for V-4Cr-4Ti alloy and V-4Cr-4Ti-0.15Y alloy. The

irradiation hardening increased with displacement damage and appeared to be saturated at 2.5 dpa.

Hardening behavior of bulk-equivalent hardness for V-4Cr-4Ti-0.15Y alloy was similar to that for

V-4Cr-4Ti alloy. Y addition has little effect on irradiation hardening at 473 K. Watanabe et al. [17]

reported that dislocation loops were formed and no irradiation-induced Ti-CON precipitates after

2.4 MeV Cu^{2+} ion-irradiation at 473 K to 0.25 dpa. Y addition suppressed irradiation-induced

precipitation due to the reduction in interstitial impurities (so-called scavenging effect) and then

improved ductility after neutron-irradiation [3-5]. Therefore, the scavenging effect of Y addition on

the improvement of irradiation hardening is significant only in the temperature range where

irradiation-induced precipitates are dominant, and is limited above the temperature between 200 and

400 ^{o}C.

3.2. FEM modeling of unirradiated V-4Cr-4Ti alloy

The ISE can be understood by noting that large strain gradients inherent in small indentations lead to geometrically necessary dislocations (GNDs) that cause enhanced hardening. To explain the ISE, Nix and Gao developed a model based on the concept of GND [7]. In the Nix-Gao model, the density of GNDs is derived from the total line length λ of dislocation loops, necessary to form the shape of a conical indenter. The total line length is then divided by a hemispherical volume V given by the contact radius a. The density of GNDs is predicted as follows:

$$\rho_G = \frac{\lambda}{V} = \frac{\dfrac{\pi h a}{b}}{\dfrac{2}{3}\pi a^3} = \frac{3}{2bh}\tan^2\theta \quad (3)$$

where b is the magnitude of Burgers vector (0.26 nm for vanadium), h is the indentation depth and θ is the angle between the surface and the indenter ($\tan\theta = h/a$, $\tan 19.7^\circ = 0.358$). The Taylor dislocation model [18] gives the shear stress τ in terms of the total dislocation density ρ_T by

$$\tau = \alpha\mu b\sqrt{\rho_T} = \alpha\mu b\sqrt{\rho_S(\varepsilon_{pl}) + \rho_G(1/h)} \quad (4)$$

where α is an empirical material constant (Tayler coefficient) between 0.1 and 0.5. μ is the shear modulus (46.7 GPa for vanadium). $\rho_S(\varepsilon_{pl})$ is the density of statistically stored dislocations (SSDs). SSDs are created by homogeneous strain and then $\rho_S(\varepsilon_{pl})$ increase as a function of plastic strain ε_{pl}. In polycrystalline specimens, the tensile flow stress σ is related to the shear stress τ by

$$\sigma = M\tau = \sqrt{\sigma_0^2(\varepsilon_{pl}) + \frac{3}{2}M^2\alpha^2\mu^2 b\left(\frac{1}{h}\right)\tan^2\theta} = \sqrt{\sigma_0^2(\varepsilon_{pl}) + 1.0\times10^3\times\alpha^2\left(\frac{1}{h}\right)} \quad (5)$$

where $\sigma_0(\varepsilon_{pl}) = M\alpha\mu b\{\rho_S(\varepsilon_{pl})\}^{1/2}$. *M* is the Taylor factor, which is set to *M* = 3.06 as suggested by

Stoller and Zinkle [19]. Since the density of GNDs is zero in uniaxial tension, σ_0 is equivalent to

constitutive equation (1). Constitutive equation (5) accounts for strain gradient dependence due to

the density of GNDs.

Figure 6 plots experimental and analytic depth profiles of hardness of unirradiated

V-4Cr-4Ti alloy. Four type FEM analyses whose constitutive equations were set to be α = 0.28, 0.5,

0.57 and No GNDs (ρ_G = 0) were carried out. Here a change in a value of α influences the density

of GNDs due to the size of plastic zone, which is a hemispherical volume V_{PZ} [20]. Adding the

concept of GNDs to constitutive equation, the ISE was simulated. FEM analysis of constitutive

equation with α = 0.5 agree well with the experimental data. A constant value of α = 0.5 is chosen

to simulate nanoindentation test for ion-irradiated V-4Cr-4Ti alloy.

3.3. FEM modeling of ion-irradiated V-4Cr-4Ti alloy

Figure 7 summarizes the increase in yield stress (YS) for neutron-irradiated V-4Cr-4Ti

alloys. Open symbols show the data for US832665 heat, which is a V-4Cr-4Ti alloy procured by the

US Department of Energy [21]. Their tensile properties for US832665 heat tested at irradiation

temperature of around 373 K were reported [22-25]. Closed square shows our data for

NIFS-HEAT-2 tested at room temperature. All the data for neutron-irradiated V-4Cr-4Ti alloys

exhibited pronounced flow localization, with uniform elongations (UE) < 0.2 % in all cases. YSs

after irradiation to 0.5 dpa at 373-603 K were independent of the irradiation temperatures [23]. The

similarity of YSs of V-4Cr-4Ti alloy irradiated at 603 K to 4-6 dpa [25] and 18 dpa [26] implies that

the irradiation hardening at this relatively low temperature (< 673 K) has reached a saturation level

already at a dose of ~5 dpa. It is assumed that a fitting expression for irradiation hardening is the

equation; $\Delta\sigma_y = \Delta\sigma_{ys}[1\text{-exp}(-\phi/\phi_0)]^{1/2}$, which is the so-called Makin-Minter model [27]. Here $\Delta\sigma_{ys}$ is

the saturation hardening, ϕ is irradiation dose and ϕ_0 specifies the dose transient prior to saturation.

Based on the experimental data for neutron-irradiated V-4Cr-4Ti alloys, the dose dependence of

irradiation hardening $\Delta\sigma_{irrad.}$ was estimated by Makin-Minter model as follows:

$$\Delta\sigma_{irrad} = 691\sqrt{1-\exp\left(-\phi/2.72\right)} \quad (6)$$

Depth profiles of irradiation hardening were determined by a combination between equation (6) and

a depth profile of ion-irradiation dose from SRIM calculation, as shown in Fig. 8.

Adding the term of irradiation hardening $\Delta\sigma_{irrad.}$ to constitutive equation with $\alpha = 0.5$, FEM

analyses for irradiated surface of V-4Cr-4Ti alloy were carried out to compare depth profiles of

nanoindentation hardness for ion-irradiated V-4Cr-4Ti alloy. Assuming Young modulus E and strain

hardening exponent n are unchanged after irradiation, the constitutive equation for irradiated

materials is described as follows:

$$\sigma = \sqrt{\sigma_0^2(\varepsilon_{pl}) + 255\left(\frac{1}{h}\right)} + \Delta\sigma_{irrad.} \quad (7)$$

Figure 9 shows comparison between the measured hardness for ion-irradiated V-4Cr-4Ti

alloy and the simulated hardness for irradiated surface of V-4Cr-4Ti alloy. FEM analyses simulated

the dose dependence of irradiation hardening. However, the dose dependence of the simulated hardness showed different trends than that of the measured hardness. The analytic data of FEM analyses based on neutron-irradiation hardening equivalent to 3.0 dpa agreed with the experimental data to 0.76 dpa. The comparison indicates that irradiation hardening by heavy ion-irradiation is larger than that by neutron-irradiation at the same displacement damage level. Possible mechanisms for extra hardening by heavy ion-irradiation are the processes that the injected Cu ions could effectively produce irradiation defects such as interstitials compared with neutrons, and that higher damage rate of ion-irradiation enhanced nucleation of irradiation defects and hence increased the number density of the defects compared with neutron-irradiation.

5. Conclusions

Irradiation hardening for ion-irradiated V-4Cr-4Ti and V-4Cr-4Ti-0.15Y alloys has been clarified by nanoindentation techniques. A comparison between nanoindentation test results and finite element method (FEM) analysis estimated depth profiles of irradiation hardening in the shallow depth for the ion-irradiated materials. It discussed the correlation between neutron-irradiation and heavy ion-irradiation from the viewpoint of mechanical strength.

For the unirradiated vanadium alloys, the indentation size effect (ISE) was clearly observed. After irradiation, irradiation hardening in the measured depth was identified. Hardening behavior of

bulk-equivalent hardness for V-4Cr-4Ti-0.15Y alloy was similar to that for V-4Cr-4Ti alloy. Y addition has little effect on irradiation hardening at 473 K.

Adding the concept of geometrically necessary dislocations (GNDs) to constitutive equation of V-4Cr-4Ti alloy, the ISE was simulated. A constant value of $\alpha = 0.5$ was derived as an optimal value to simulate nanoindentation test for ion-irradiated V-4Cr-4Ti alloy. Adding the term of irradiation hardening $\Delta\sigma_{irrad.}$ to constitutive equation with $\alpha = 0.5$, FEM analyses for irradiated surface of V-4Cr-4Ti alloy were carried out. The analytic data of FEM analyses based on neutron-irradiation hardening equivalent to 3.0 dpa agreed with the experimental data to 0.76 dpa. The comparison indicates that irradiation hardening by heavy ion-irradiation is larger than that by neutron-irradiation at the same displacement damage level.

Acknowledgements

References

1. S.J. Zinkle, H. Matsui, D.L. Smith, A.F. Rowcliffe, E. van Osch, K. Abe and V.A. Kazakov, J. Nucl. Mater. 258-263 (1998) 205-214.

2. A.F. Rowcliffe, S.J Zinkle and D.T. Hoelzer, J. Nucl. Mater. 283-287 (2000) 508-512.

3. M. Satou, T. Chuto and K. Abe, J. Nucl. Mater. 283-287 (2000) 367-371.

4. T. Chuto, M. Satou and K. Abe, J. Nucl. Mater. 283-287 (2000) 503-507.

5. T. Chuto, M. Satou, A. Hasegawa, K. Abe, T. Muroga and N. Yamamoto: ASTM STP 1447 (2004) 693.

6. C. Abromeit, J. Nucl. Mater. 216 (1994) 78-96.

7. W.D. Nix and H. Gao, J. Mech. Phys. Solids. 46 (1998) 411-425.

8. Y. Takayama, R. Kasada, Y. Sakamoto, K. Yabuuchi, A. Kimura, M. Ando, D. Hamaguchi and H. Tanigawa, J. Nucl. Mater. 442 (2013) S23-S27.

9. T. Nagasaka, T. Muroga, M. Imamura, S. Tomiyama and M. Sakata, Fusion Technol. 39, (2001) 659-663.

10. T. Nagasaka, T. Muroga, T. Hino, M. Satou, K. Abe, T. Chuto and T. Iikubo, J. Nucl. Mater. 367-370 (2007) 823-828.

11. http://www.srim.org/

12. ASTM E521-96 (2003), Standard Practice for Neutron Radiation Damage Simulation by Charged Particle Irradiation. Annual Book of ASTM Standards, vol. 12.02.

13. W.C. Oliver and G.M. Pharr, J. Mater. Res. 7 (1992) 1564.

14. J.A. Knapp, D.M. Follstaedt, S.M. Myers, J.C. Barbour and T.A. Friedmann, J. Appl. Phys. 85 (1999) 1460.

15. H.W. Swift, J. Mechanics and Physics of Solids. 1 (1952) 1-18.

16. A. Nishimura, T. Nagasaka and T. Muroga, J. Nucl. Mater. 307-311 (2002) 571-575.

17. H. Watanabe, T. Arinaga, K. Ochiai, T. Muroga and N. Yoshida, J. Nucl. Mater. 283-287 (2000) 286-290.

18. G.I. Taylor, J. Inst. Metals, 62 (1938) 307-324.

19. R.E. Stoller and S.J. Zinkle, J. Nucl. Mater. 283-287 (2000) 349-352.

20. K. Durst, B. Backes and M. Goken, Script. Mater. 52 (2005) 1093-1097.

21. T.S. Bray, H. Tsai, L.J. Nowicki, M.C. Billone, D.L. Smith, W.R. Johnson and P.W. Trester, J. Nucl. Mater. 283-287 (2000) 633-636.

22. A.N. Gubbi, A.F. Rowcliffe, W.S. Eatherly and L.T. Gibson, Fusion Materials Semiannual. Prog. Report for period ending 30 June 1996, DOE/ER-0313/20, p.38.

23. L.L. Snead, S.J. Zinkle, D.J. Alexander, A.F. Rowcliffe, J.P. Robertson and W.S. Eatherly, Fusion Materials Semiannual. Prog. Report for period ending 31 December 1997, DOE/ER-0313/23, p.81.

24. H. Bohm, in: International Symposium on Effects of Radiation on Structural Materials, ASTM STP 426, American Society for Testing and Materials, Philadelphia, 1966, p. 95..

25. E.V. van Osch and M.I. de Vries, J. Nucl. Mater. 271&272 (1999) 162-166.

26. V.A. Kazakov, V.P. Chakin and Yu.D. Goncharenko, J. Nucl. Mater. 258-263 (1998) 1492-1496.

27. M.J. Makin and F.J. Minter, Acta. Metall. 8 (1960) 691-699.

28. J.F. Smith, Phase Diagrams of Binary Vanadium Alloys, ASM INTERNATIONAL, (1989).
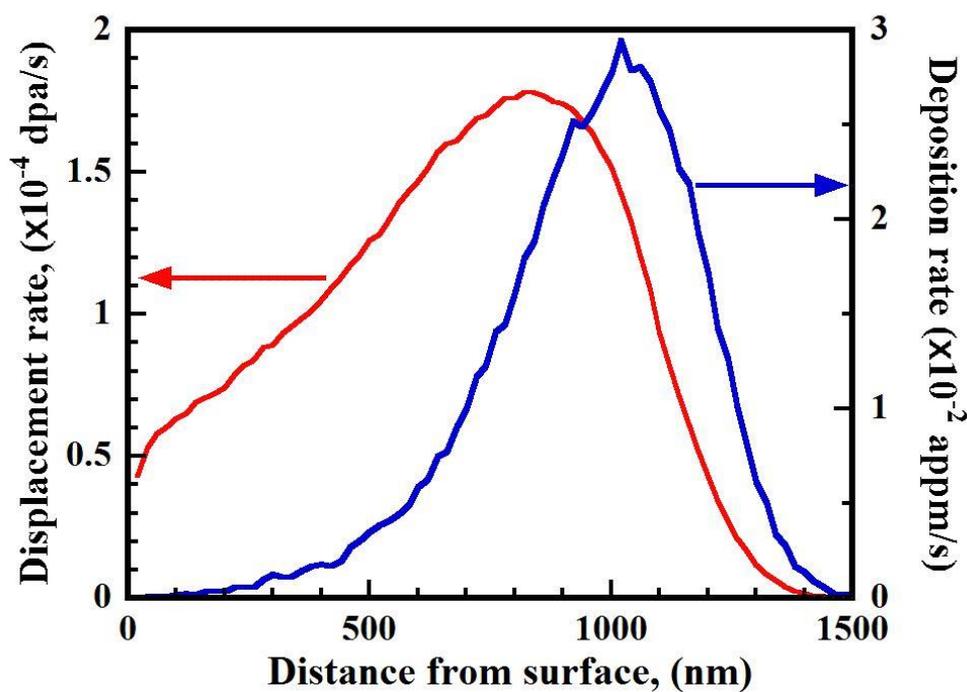
Figure captions:

Fig. 1. Depth profiles of displacement rate and Cu ions deposition rate calculated for the investigated irradiation conditions.

Fig. 2. Uniaxial true stress-true plastic strain curves of V-4Cr-4Ti alloy tested at room temperature at an initial strain rate of 0.05 s^{-1}.

Fig. 3. Depth profiles of nanoindentation hardness for (a) V-4Cr-4Ti alloy and (b) V-4Cr-4Ti-0.15Y alloy.

Fig. 4. Plots of H^2 versus $1/h$ for (a) V-4Cr-4Ti alloy and (b) V-4Cr-4Ti-0.15Y alloy.

Fig. 5. Dose dependence of bulk-equivalent hardness for (a) V-4Cr-4Ti alloy and (b) V-4Cr-4Ti-0.15Y alloy.

Fig. 6. Experimental and analytic depth profiles of hardness of unirradiated V-4Cr-4Ti alloy.

Fig. 7. The increase in yield stress (YS) for neutron-irradiated V-4Cr-4Ti alloys. Open symbols show the data for US832665 heat tested at irradiation temperature of around 373 K [22-25]. Closed square shows the data for NIFS-HEAT-2 tested at room temperature. The curve were fit to the dose dependence of the increase in YS using $\Delta\sigma_y = \Delta\sigma_{ys}[1-\exp(-\phi/\phi_0)]^{0.5}$.

Fig. 8. Depth profiles of irradiation hardening determined by a combination between Makin-Minter model and SRIM calculation.

Fig. 9. Comparison between the measured hardness for ion-irradiated V-4Cr-4Ti alloy and the simulated hardness for irradiated surface of V-4Cr-4Ti alloy.

Figures:

Fig. 1. Depth profiles of displacement rate and Cu ions deposition rate calculated for the
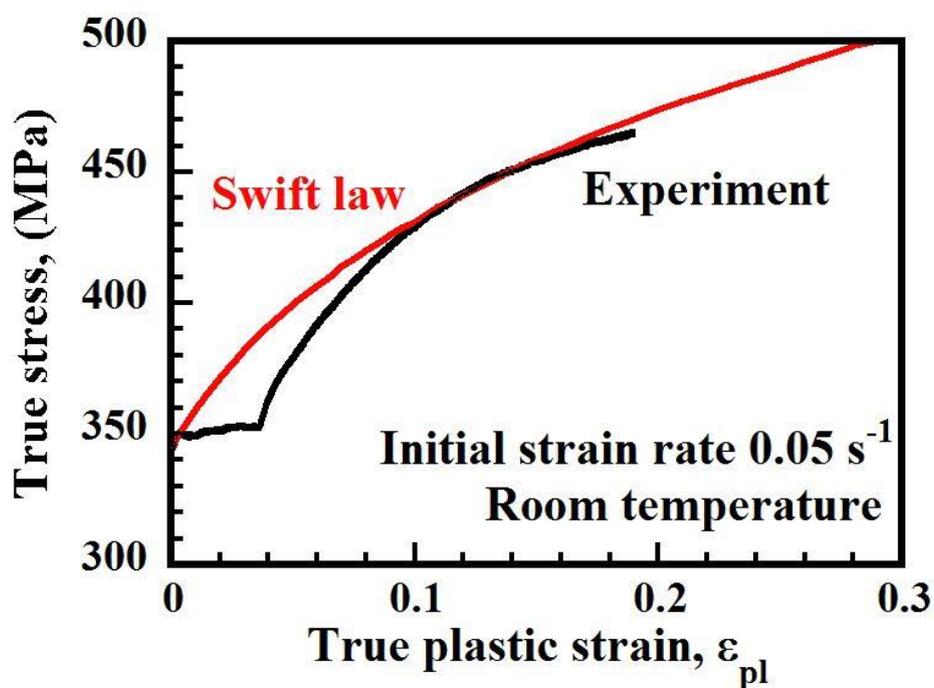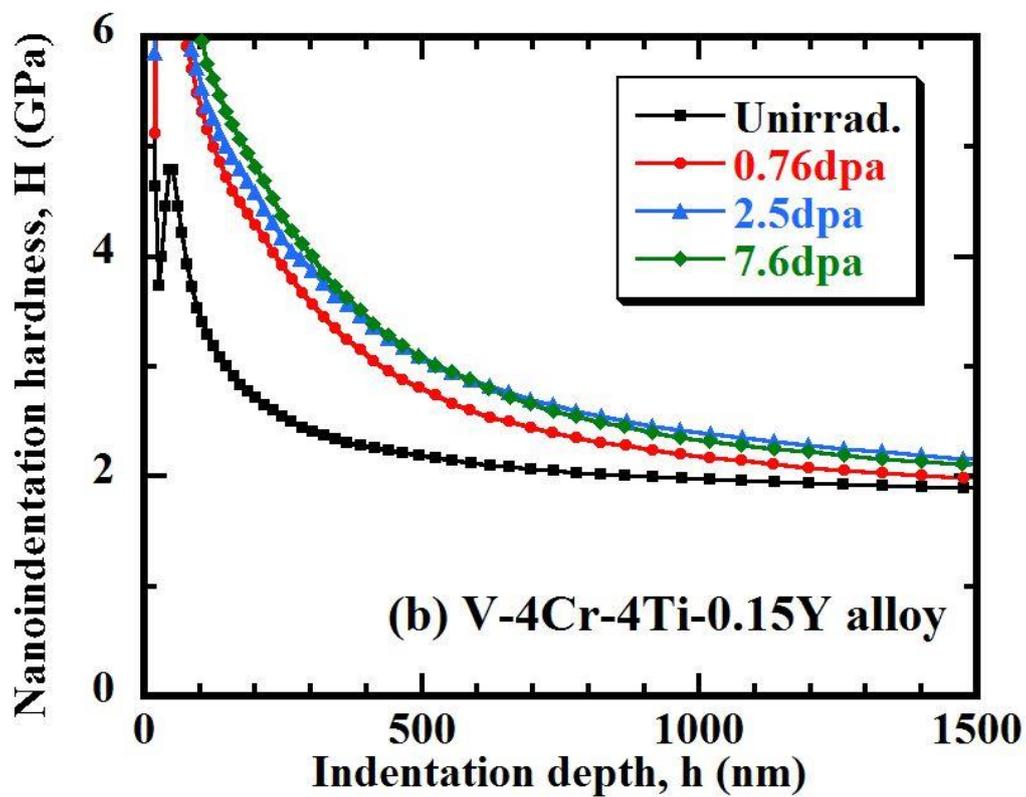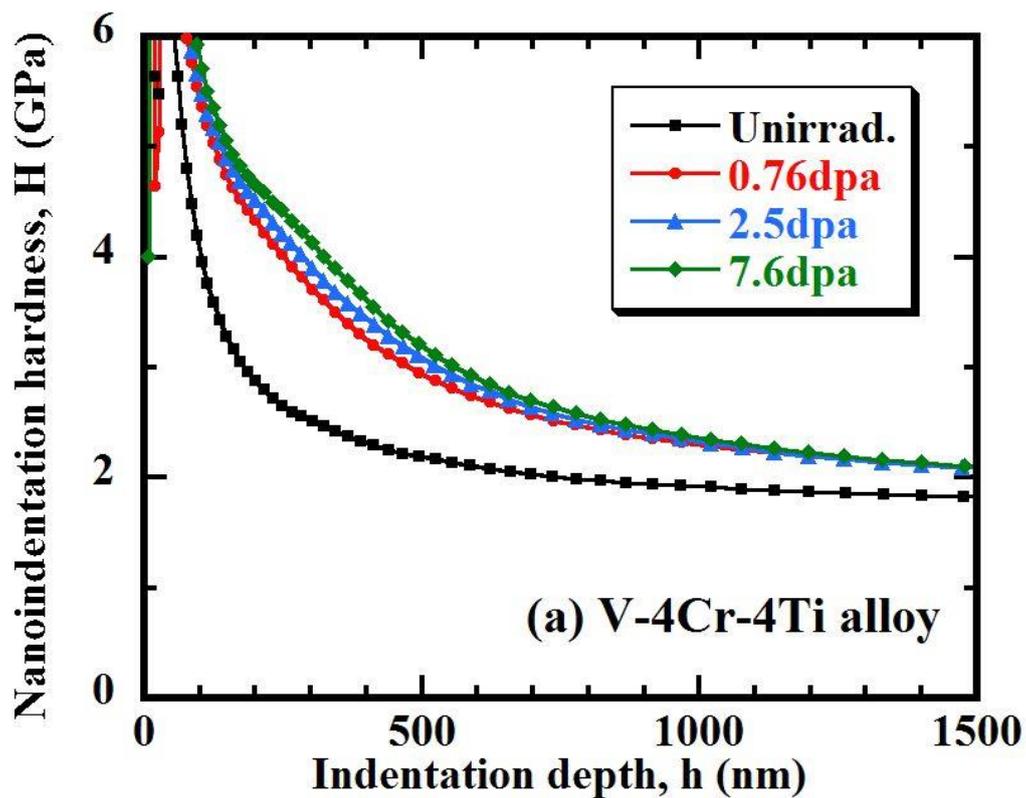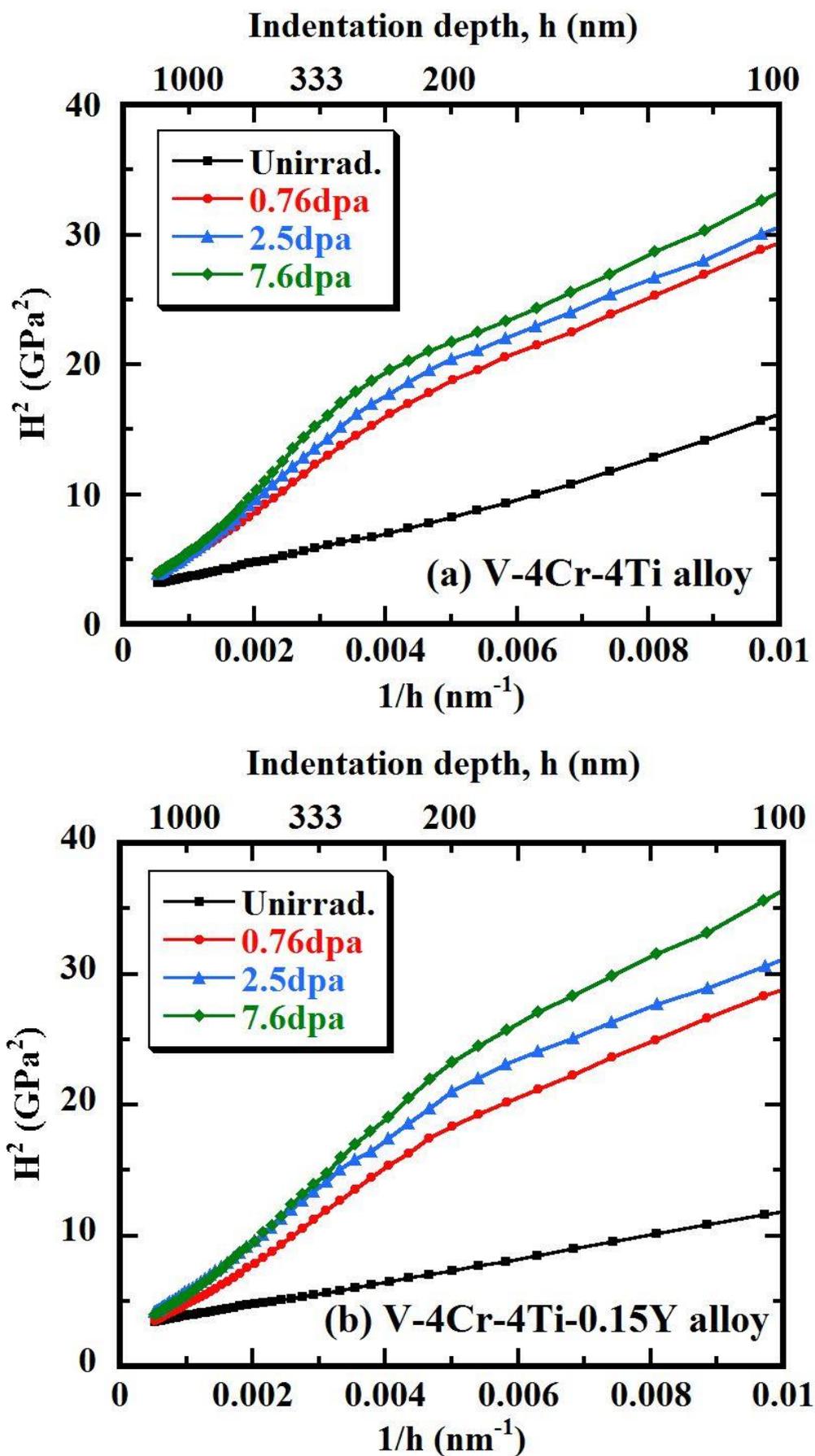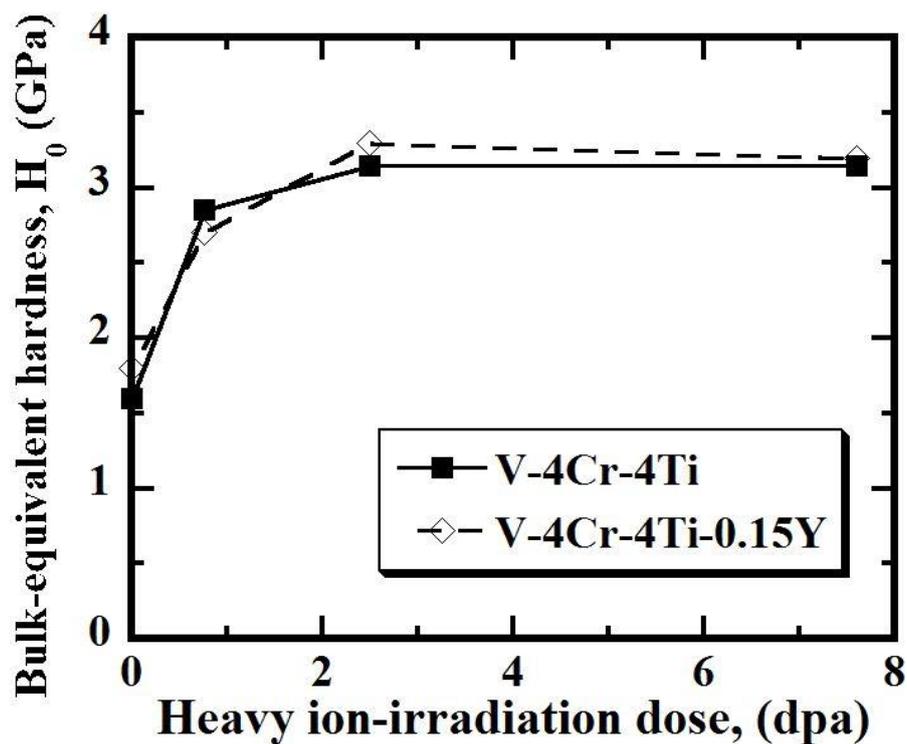
investigated irradiation conditions.

Fig. 2. Uniaxial true stress-true plastic strain curves of V-4Cr-4Ti alloy tested at room temperature

at an initial strain rate of 0.05 s^{-1}.

Fig. 3. Depth profiles of nanoindentation hardness for (a) V-4Cr-4Ti alloy and (b) V-4Cr-4Ti-0.15Y

alloy.

Fig. 4. Plots of H^2 versus $1/h$ for (a) V-4Cr-4Ti alloy and (b) V-4Cr-4Ti-0.15Y alloy.

Fig. 5. Dose dependence of bulk-equivalent hardness for (a) V-4Cr-4Ti alloy and (b)
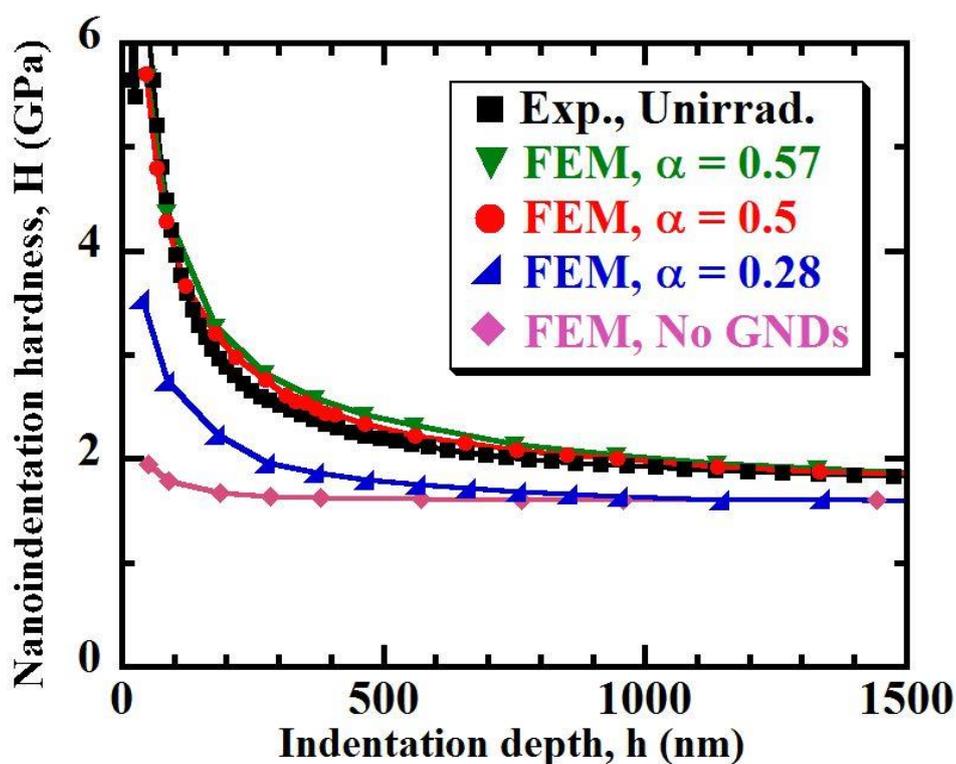
V-4Cr-4Ti-0.15Y alloy.

Fig. 6. Experimental and analytic depth profiles of hardness of unirradiated V-4Cr-4Ti alloy.
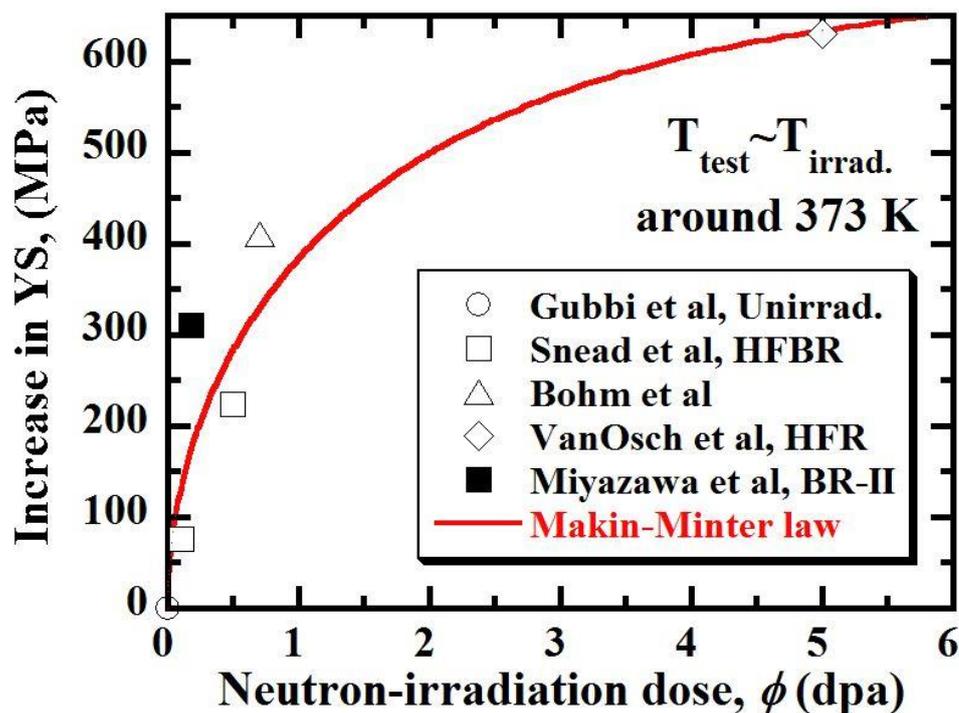
Fig. 7. The increase in yield stress (YS) for neutron-irradiated V-4Cr-4Ti alloys. Open symbols show the data for US832665 heat tested at irradiation temperature of around 373 K [22-25]. Closed square shows the data for NIFS-HEAT-2 tested at room temperature. The curve were fit to the dose dependence of the increase in YS using $\Delta\sigma_y = \Delta\sigma_{ys}[1-\exp(-\phi/\phi_0)]^{0.5}$.
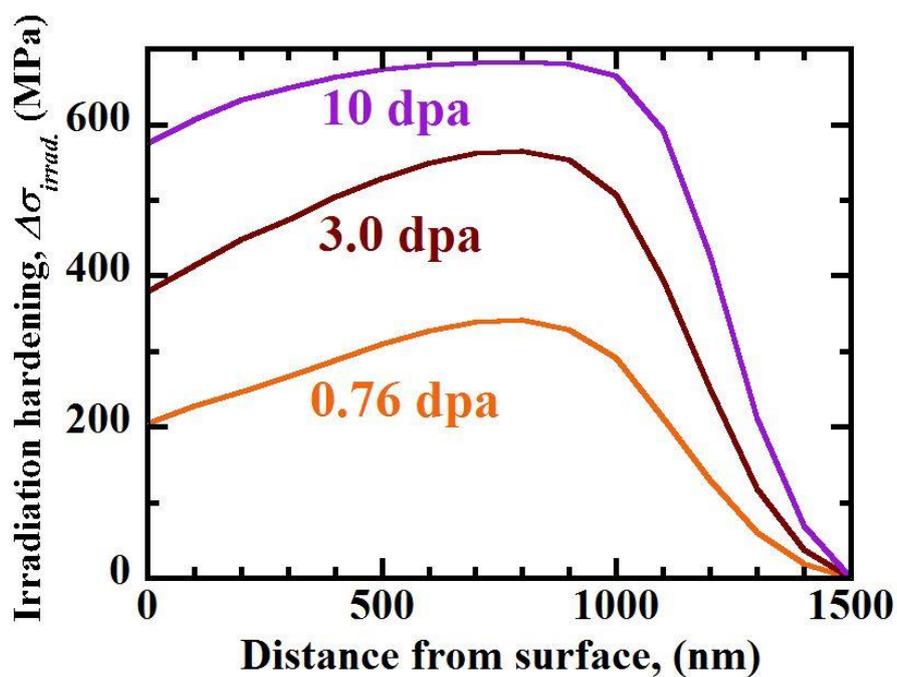
Fig. 8. Depth profiles of irradiation hardening determined by a combination between Makin-Minter
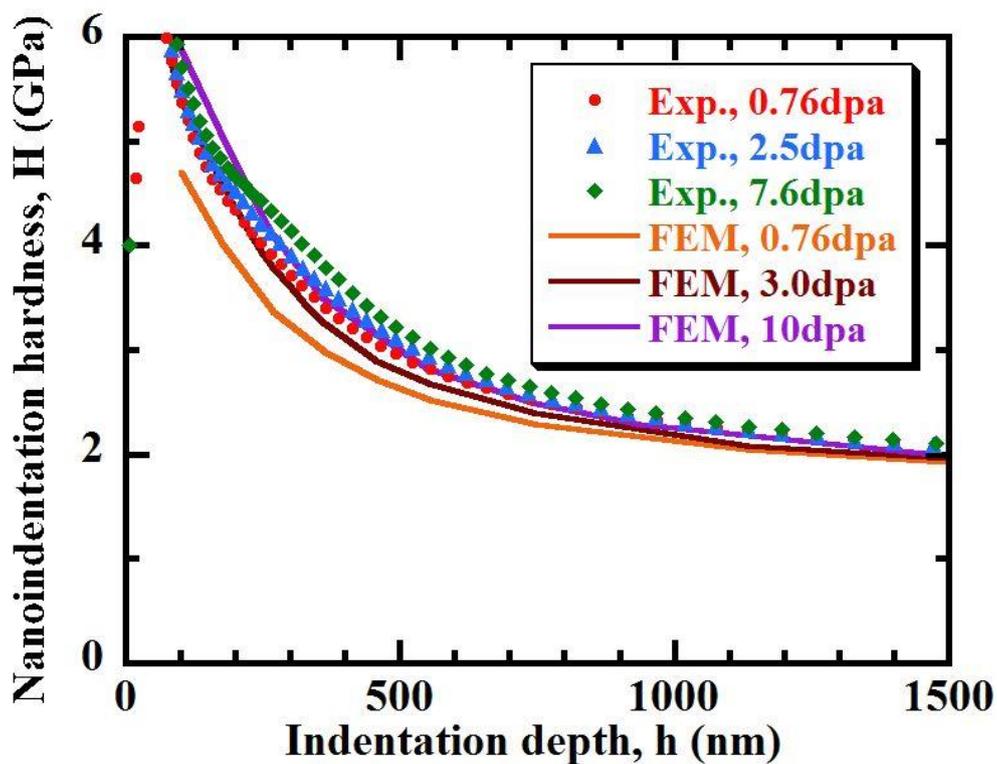
model and SRIM calculation.

Fig. 9. Comparison between the measured hardness for ion-irradiated V-4Cr-4Ti alloy and the

simulated hardness for irradiated surface of V-4Cr-4Ti alloy.